 CMC, vol.27, no.1, pp.23-53, 2012

A New Optimized Algorithm with Nonlinear Filter for Ultra-Tightly Coupled Integrated Navigation System of Land Vehicle

Chien-Hao Tseng[1], Dah-Jing Jwo[2] and Chih-Wen Chang[1]

Abstract: The extended particle filter (EPF) assisted by the Takagi-Sugeno (T-S) fuzzy logic adaptive system (FLAS) is used to design the ultra-tightly coupled GPS/INS (inertial navigation system) integrated navigation, which can maneuver the vehicle environment and the GPS outages scenario. The traditional integrated navigation designs adopt a loosely or tightly coupled architecture, for which the GPS receiver may lose the lock due to the interference/jamming scenarios, high dynamic environments, and the periods of partial GPS shading. An ultra-tight GPS/INS architecture involves the integration of I (in-phase) and Q (quadrature) components from the correlator of a GPS receiver with the INS data. The EPF is a particle filter (PF) which uses the extended Kalman filter (EKF) to generate the proposal distribution. The PF depends mostly on the number of particles in order to achieve a better performance during the high dynamic environments and GPS outages. The T-S FLAS is one of these approaches that can prevent the divergence problem of the filter when the precise knowledge on the system models is not available. The results show that the proposed fuzzy adaptive EPF (FAEPF) can effectively improve the navigation estimation accuracy and reduce the computational load as compared with the EPF and the unscented Kalman filter (UKF).

Keywords: Ultra-tightly coupled, Fuzzy logic, Extended Kalman filter (EKF), Unscented Kalman filter (UKF), Extended particle filter (EPF)

1 Introduction

Recently, some researchers are involved in the ultra-tightly coupled GPS/INS integrated navigation system due to the fact that the conventional passive integra-

[1] Computing Technology Integration Division, National Center for High-Performance Computing, Taichung 40763, Taiwan

[2] Department of Communications, Navigation and Control Engineering, National Taiwan Ocean University, Keelung 20224, Taiwan. Author to whom correspondence should be addressed, E-mail: djjwo@mail.ntou.edu.tw

tion systems are highly susceptible to the signal interference and/or jamming distortions. There are various architectures for integrating the GPS with INS [Salychev (1998)]. The traditional GPS/INS integration designs use a loosely or tightly coupled architecture. The loosely coupled integration uses the GPS to derive the position and the velocity as measurements. To prevent GPS outages, the loosely coupled integration is a sub-optimal architecture (i.e., when using less than four available satellites). A tightly coupled GPS/INS navigation filter blends the GPS pseudorange, the inertial measurements and obtains the vehicle navigation solution [Farrell and Barth (1999)]. The ultra-tightly coupled architecture combines the I (in-phase) and Q (quadrature) correlator components in the receiver signal tracking loops and the INS navigation filter function as a single integrated filter.

In the ultra-tightly coupled integration mode, the correlator variables I/Q and the INS states formed the error states which are given as measurements to the integration filter [Yu, Wang and Ji (2010)]. The integration filter estimates the inertial errors and bias offsets. The inherent property of this system is the integration of INS derives Doppler feedback to the carrier tracking loops. Babu and Wang (2004) mentioned the advantage of INS Doppler aiding removes the vehicle Doppler from the GPS signal, which facilitates a significant reduction in the carrier tracking loop bandwidth and periods of the partial GPS shading on a comparative scale the dynamics on the pseudorandom noise (PRN) code is slight due to its low frequency. The bandwidth reduction improves the anti-jamming performance of the receiver, and also increases the post correlated signal strength [Wang and Li (2011)]. In addition, the accuracy of the raw measurements also increases due to the lower bandwidths.

If the estimation is not accurate, it may cause the system instability and the loss of lock. Thus, the design of navigation filter is one of the important tasks in the ultra-tightly coupled GPS/INS integration. In the current integration scenarios, the extended Kalman filter (EKF) and the unscented Kalman filter (UKF) are employed to implement the ultra-tight system [Babu and Wang (2009), Yuan and Zhang (2009)]. Theses Kalman filtering techniques suffer from the divergence during the GPS signal blockages due to approximations during linearization process and the system miss-modeling [Noureldin, Karamat, Eberts and El-Shafie (2009)]. The EKF also results in the high computational load owing to the Jacobian matrices evaluations, i.e. from the linear approximations to the nonlinear functions [Julier, Uhlmann and Durrant (2000)]. Moreover, these small error tolerances of EKF can cause the inconsistency of the covariance update and lead to the filter instability or the divergence [Lerro and Shalom (1995)].

To overcome shortcomings of EKF, the popular alternatives include the UKF [Julier, Uhlmann and Durrant (1995)] and PF [Won, Melek and Golnaraghi (2010)]. The

UKF approximates the Gaussian distribution by a set of deterministically selected samples called the sigma points, which are propagated through the true non-linear models to capture the true mean and the covariance of the transformed distribution. Nevertheless, when the non-linearity is highly prominent, both the EKF and UKF assume the noise is Gaussian distribution, which is a poor approximation to the posterior distribution [Doucet, Godsill and Andrieu (2000), Doucet, Freitas and Gordon (2001)] for highly nonlinear systems. To tackle these problems, the extended particle filter (EPF) was proposed to approximate the posterior distribution for highly nonlinear systems, which was a non-parametric filter and dealt with nonlinear and/or non-Gaussian noises easily. The EKF is used to generate the proposal distribution for acquiring a maximum a posteriori probability. Besides, the important density function can approximate the true posterior density distribution. The important proposal distribution integrates the latest observation into the system state transition density so as to match the posteriori density properly. However, the particle filter requires an impractically large number of particles to sample the state space effectively; otherwise, it is easy to lose the track and inaccuracy when estimating the weights because the sample depletion is in the state space.

To improve the above-mentioned problems, we propose the fuzzy adaptive EPF with the T-S fuzzy logic adaptive system (FLAS) to cope with the low computation load and the high accurate of estimations under the maneuvering environments and periods of the partial GPS signal outages [Boucher and Noyer (2010)]. The uncertainty of process noise and measurement noise will degrade the performance of EPF. To deal with the noise uncertainty and the system nonlinearity simultaneously, the fuzzy reasoning system is constructed of obtaining the suitable process noise according to the time-varying change in dynamics. By monitoring the innovation information, we use the FLAS to determine the process noise covariance according to the innovation information so as to obtain the accurate estimation and tracking capability. The results show that the fuzzy adaptive EPF scheme can remarkably improve the accuracy of navigation estimation during GPS outages and the maneuvering environments. In addition, it can successfully reduce the computational cost.

This paper is organized as follows. In Section 2, the preliminary background of the nonlinear filters is briefly reviewed and the basic concept of PF and EPF algorithms are presented. The ultra-tightly coupled integrated navigation strategy is introduced in Section 3. Section 4 describes the proposed fuzzy logic adaptive EPF sensor fusion strategy. In Section 5, the numerical simulations and performance evaluation are carried out, and comparing the performance of the proposed FAEPF method with the relatively conventional EPF and UKF approaches. Some important remarks from the present research are summarized in Section 6.

2 The nonlinear filters

In the decades, the nonlinear filtering approach has been investigated the navigation problem, but not as common as the EKF [e.g., Li, Wang, Rizos, Mumford and Ding (2006), Crassidis (2006)]. The Kalman filtering has been recognized as one of the most powerful state estimation techniques. The purpose of the Kalman filter is to provide the estimation with minimum error variance. The extended Kalman filter is a nonlinear version of the Kalman filter and is widely used to the navigation sensor fusion.

By using the nonlinear stochastic difference equations of EKF, we can deal with the case is as follows:

$$\mathbf{x}_{k+1} = \mathbf{f}(\mathbf{x}_k, \mathbf{w}_k),\ \mathbf{z}_k = \mathbf{h}(\mathbf{x}_k, \mathbf{v}_k), \tag{1}$$

where $E[\cdot]$ represents the expectation, and superscript "T" denotes the matrix transpose. The state vector $\mathbf{x}_k \in \Re^n$, the process noise vector $\mathbf{w}_k \in \Re^n$, the measurement vector $\mathbf{z}_k \in \Re^m$, and the measurement noise vector $\mathbf{v}_k \in \Re^m$. In Eq. (1), both the vectors $\mathbf{w}_k$ and $\mathbf{v}_k$ are the zero mean Gaussian white sequences having the zero cross correlation with each other:

$$\mathbf{E}[\mathbf{w}_k \mathbf{w}_i^{\mathrm{T}}] = \begin{cases} \mathbf{Q}_k, & i = k \\ 0, & i \neq k \end{cases}, \quad \mathbf{E}[\mathbf{v}_k \mathbf{v}_i^{\mathrm{T}}] = \begin{cases} \mathbf{R}_k, & i = k \\ 0, & i \neq k \end{cases}, \quad \mathbf{E}[\mathbf{w}_k \mathbf{v}_i^{\mathrm{T}}] = \mathbf{0}, \quad for\ all\ i\ and\ k, \tag{2}$$

where $\mathbf{Q}_k$ is the process noise covariance matrix, and $\mathbf{R}_k$ is the measurement noise covariance matrix.

The EKF is the first of the approximate nonlinear filters, which linearizes the system and measurement equations about a single sample point with the assumption that the a priori distribution is Gaussian. The Kalman filter algorithm starts with an initial condition value, the state vector $\bar{\mathbf{x}}_0$ and the state covariance matrix $\bar{\mathbf{P}}_0$. When the new measurement $\mathbf{z}_k$ becomes available with the progression of time, the estimation of states and the corresponding error covariance would follow recursively ad infinity. Further detailed discussion of EKF can be referred to [Brown and Hwang (1997), Gelb (1997)].

2.1 The unscented Kalman filter

The UKF was first proposed by Julier, Uhlmann and Durrant (1995). Instead of linearizing Jacobian matrices in the EKF and achieving first-order accuracy, the UKF uses a deterministic sampling approach to capture the mean and covariance

estimates with a minimal set of sample points (weighted samples). The state distribution of EKF is approximated by a Gaussian random variable (GRV), which is then propagated analytically through the first-order linearization of the nonlinear system.

The first step in the UKF is to sample the prior state distribution, i.e. to generate the sigma points through the unscented transformation (UT) [Julier (2002), Julier and Uhlmann (2002)]. By employing the UT method to calculate the statistics of a random variable, and it needs a nonlinear transformation. However, using a probability distribution is easier than to approximate an arbitrary nonlinear transformation. A set of sigma points is deterministically chosen so as to capture the true mean and covariance of the random variable. The samples are propagated through true nonlinear equations, and the model is not linearized. The UKF generates these sigma points about the mean estimate. The UKF works on the principle that a set of discretely sampled sigma points can be used to parameterize the mean and covariance of GRVs. Then, the posterior mean and covariance are propagated through the true nonlinear function without the linearized steps. The UKF requires a little computational cost due to the deterministic sampling of sigma points as opposed to the random particles of particle filter [Gordon, Ristic and Arulampalam (2004)]. The flow chart of UKF approach is summarized:

1) The transformed set is given by instantiating each point through the process model:

$$(\bar{\zeta}_k)_i = f((\bar{\mathbf{X}}_k)_i). \tag{3}$$

2) Predicted mean

$$\bar{\mathbf{x}}_k = \sum_{i=0}^{2n} W_i^{(m)} (\bar{\zeta}_k)_i. \tag{4}$$

3) Predicted covariance

$$\bar{\mathbf{P}}_k = \sum_{i=0}^{2n} W_i^c [(\bar{\zeta}_k)_i - \bar{\mathbf{x}}_k][(\bar{\zeta}_k)_i - \bar{\mathbf{x}}_k]^T + \mathbf{Q}_k. \tag{5}$$

4) Instantiate each of the prediction points through observation model:

$$(\bar{\mathbf{Z}}_k)_i = \mathbf{h}((\bar{\zeta}_k)_i). \tag{6}$$

5) Predicted observation

$$\bar{\mathbf{z}}_k = \sum_{i=0}^{2n} W_i^{(m)} (\bar{\mathbf{Z}}_k)_i. \tag{7}$$

6) Innovation covariance

$$\mathbf{P}_{\mathrm{yy}} = \sum_{i=0}^{2n} W_i^{(c)} [(\bar{\mathbf{Z}}_k)_i - \bar{\mathbf{z}}_k][(\bar{\mathbf{Z}}_k)_i - \bar{\mathbf{z}}_k]^T + \mathbf{R}_k. \tag{8}$$

7) Cross covariance

$$\mathbf{P}_{\mathrm{xz}} = \sum_{i=0}^{2n} W_i^{(c)} [(\bar{\zeta}_k)_i - \bar{\mathbf{x}}_k][(\bar{\mathbf{Z}}_k)_i - \bar{\mathbf{z}}_k]^T. \tag{9}$$

8) Performing update using the nominal KF

$$\mathbf{K}_k = \mathbf{P}_{\mathrm{xz}} \mathbf{P}_{\mathrm{yy}}^{-1}, \tag{10}$$

$$\hat{\mathbf{x}}_k = \bar{\mathbf{x}}_k + \mathbf{K}_k(\mathbf{z}_k - \bar{\mathbf{z}}_k), \tag{11}$$

$$\mathbf{P}_k = \bar{\mathbf{P}}_k - \mathbf{K}_k \mathbf{P}_{\mathrm{yy}} \mathbf{K}_k^T. \tag{12}$$

2.2 The generic particle filter

The sequential importance sampling (SIS) is one of the Monte Carlo methods, which implements the Bayesian estimation by Monte Carlo simulation. The idea of SIS uses the samples with weights to approximate the posterior $p(\mathbf{X}_k|\mathbf{Y}_k)$. When the number of samples is infinite, the approximated approaches are the true posterior density [Arulampalan, Maksell, Gordon and Clapp (2002)]. The key idea is to represent the required posterior density function by a set of random samples with the associated weights and to compute estimates on the basis of these samples and weights.

Let $\{\mathbf{X}_k^i,\ \omega_k^i\}_{i=1}^N$ denote a random measure that characterizes the joint posterior probability distribution function (pdf) $p(\mathbf{X}_k|\mathbf{Y}_k)$. Here $\{\mathbf{X}_k^i, i = 1,..., N\}$ are the particles with weights $\{\omega_k^i, i = 1,...,N\}$. The weights are normalized such that $\sum_i \omega_k^i = 1$. At k step, the posterior density can be approximated as

$$p(\mathbf{X}_k|\mathbf{Y}_k) \approx \sum_{i=1}^{N} \omega_k^i \delta(\mathbf{X}_k - \mathbf{X}_k^i), \tag{13}$$

where

$$\omega_k^i \propto \omega_{k-1}^i \frac{p(\mathbf{y}_k|\mathbf{x}_k^i) p(\mathbf{x}_k^i|\mathbf{x}_{k-1}^i)}{q(\mathbf{x}_k^i|\mathbf{x}_{k-1}^i, \mathbf{y}_k)}, \tag{14}$$

where $p(\mathbf{y}_k|\mathbf{x}_k^i)$ is the likelihood function of the measurements $\mathbf{y}_k$, $p(\mathbf{x}_k^i|\mathbf{x}_{k-1}^i)$ is the prior, and $q(\mathbf{x}_k^i|\mathbf{x}_{k-1}^i,\mathbf{y}_k)$ is the importance density. To normalize Eq. (14), we can obtain

$$\omega_k^i = \frac{\omega_k^i}{\sum \omega_k^i}, \tag{15}$$

and the estimation of the posterior can be represented by:

$$p(\mathbf{x}_k|\mathbf{Y}_k) \approx \sum_{i=1}^{N} \omega_k^i \delta(\mathbf{x}_k - \mathbf{x}_k^i), \tag{16}$$

when $N \to \infty$ it can approximate the true probability density $p(\mathbf{X}_k|\mathbf{Y}_k)$.

Besides, a good proposal distribution is essential to the efficiency of importance sampling. From Eqs. (13) and (14), it is shown that the particle filter consists of the recursive propagation of weights and the support points when each measurement is received sequentially. However, the generic particle filter has a problem of the degeneracy phenomenon. The degeneracy problem may reduce accuracy of the estimation. To avoid the degeneracy phenomenon of particles, one of the accurate methods is to add the number of samples (or particles). Nevertheless, if the particle filter adds too many particles in the filter, a large computational burden will be devoted. Therefore, the resampling is a better method to reduce the degeneracy of algorithm. As for the resampling scheme, there are many selections such as the sampling importance resampling (SIR), the residual resampling and the systematic resampling. In this paper, the systematic resampling is used in all of the experiments. The corresponding pseudocode is displayed in Fig. 1.

2.3 The extended particle filter

The importance density function is used in the SIS and SIR schemes, in which the transition prior does not consider the most recent measurement data $\mathbf{y}_k$. Consequently, the deficiency may arise in the particle filters, especially when there is slight overlap between the importance density function and the posterior pdf $p(\mathbf{X}_k|\mathbf{Y}_k)$, and the estimation result is poor. To avoid this problem that may arise from using the transition prior as the importance density function, the filter needs to incorporate the latest measurement data into it. In the structure of SIR, one adds EKF algorithm into the SIR filter [Aggarwal, Gu and El-Sheimy (2007), Carpenter, Fearnhead and Clifford (1999)]. The importance weights of particles will be updated through the resampling. In this framework, each particle is generated by the EKF, which is employed to generate and propagate the importance density function. Moreover, the EKF is utilize to the proposal distribution generation within

u ~ $\mathbf{U}(0,1)/N$; where N is the number of particles.
j = 1; $l = 0$; i =0 ;
do while u < 1
  if $l >$ u then
    $u = u + 1/N$; output x^i
  else
    pick k in $\{j,....,N\}$
    $i = \mathbf{x}^k$, $l = l + \omega^i$
    switch $(\mathbf{x}^k, \omega^k)$ with $(\mathbf{x}^j, \omega^j)$
    j = j + 1
  end if
end do

Figure 1: The pseudocode for the systematic resampling.

a particle filter framework, which is called the extended particle filter (EPF). The algorithm of EPF is summarized in Fig. 2.

3 The ultra-tight GPS/INS integrated system

The ultra-tightly coupled GPS/INS integration strategy is shown in Fig. 3. The quadrature signals from the receiver correlator, in-phase (I) and quadrature (Q) components form the measurements of the filters. These I and Q measurements from channels $\{1, 2, ... N\}$ are integrated with the position, velocity and attitude of the INS in a complementary filter.

The received satellite signal can be presented as

$$y(t) = A \cdot CA(t) \cdot D(t) \cos(2\pi f_0 (t - \tau) + \theta_0) + \eta, \tag{17}$$

where A is the signal amplitude, $CA(t)$ is the C/A code sequence, $D(t)$ is the navigation data, τ is the propagation delay between the satellite and the receiver, f_0 is the carrer frequency, θ_0 is the initial carrer phase, and η is the Gaussian noise. Ignoring the atmospheric and oscillator effects, the propagation delay τ can be expanded as follows:

$$\tau = \frac{|P_s(t_s) - P_r(t_r)|}{c}, \tag{18}$$

(1). Initialization:

Draw particles $\mathbf{x}_0^i$ from $\mathbf{P}(x_0)$, where $i = 1 \ldots N$.

(2). EKF algorithm:

In prediction step of EKF, (1a) is rewritten as $\hat{\mathbf{x}}_k^{(-)i} = \mathbf{f}_{k-1}(\hat{\mathbf{x}}_{k-1}^i, \mathbf{w}_{k-1}^i)$. Where $\mathbf{w}_{k-1}^i$ is randomly generated on the basis of know pdf of $\mathbf{w}_{k-1}$ Sample the particles from $\mathbf{x}_k^i \sim q(\mathbf{x}_k^i \mid \mathbf{x}_{k-1}^i, \mathbf{y}_k) = N(\hat{\mathbf{x}}_k^i, \mathbf{P}_k^i)$, where $\hat{\mathbf{x}}_k^i$, $\mathbf{P}_k^i$ are the estimation of mean and covariance of EKF.

(3). The importance weights update:

$$\omega_k^i \propto \frac{p(\mathbf{y}_k \mid \mathbf{x}_k^i)\, p(\mathbf{x}_k^i \mid \mathbf{x}_{k-1}^i)}{q(\mathbf{x}_k^i \mid \mathbf{x}_{k-1}^i, \mathbf{y}_k)}$$

(4). Normalized the importance weights:

$$\omega_k^i = \frac{\omega_k^i}{\sum_{i=1}^{N} \omega_k^i}$$

(5). Resampling step:

Using systematic resampling to resample new index j

$$\mathbf{x}_k^i = \mathbf{x}_k^j$$

$$\mathbf{P}_k^i = \mathbf{P}_k^j$$

$$\omega_k^i = \frac{1}{N}$$

Figure 2: The procedure of extended particle filter algorithm.

where $P_s(t_s)$ is the satellite position at transmit time, $P_r(t_r)$ is the receiver position at receive time, $t_r = t_s + \tau$, and c is the velocity of light. Considering the motion of both the satellite and the receiver, the numerator Eq. (18) can be expanded through the Taylor's series:

$$|P_s(t_s) - P_r(t_r)| \approx |P_s(t_0 - \tau) - P_r(t_0)| + \frac{d}{dt} |P_s(t_0 - \tau) - P_r(t_0)|\,(t - t_0), \tag{19}$$

where t_0 is the time at a reference point.

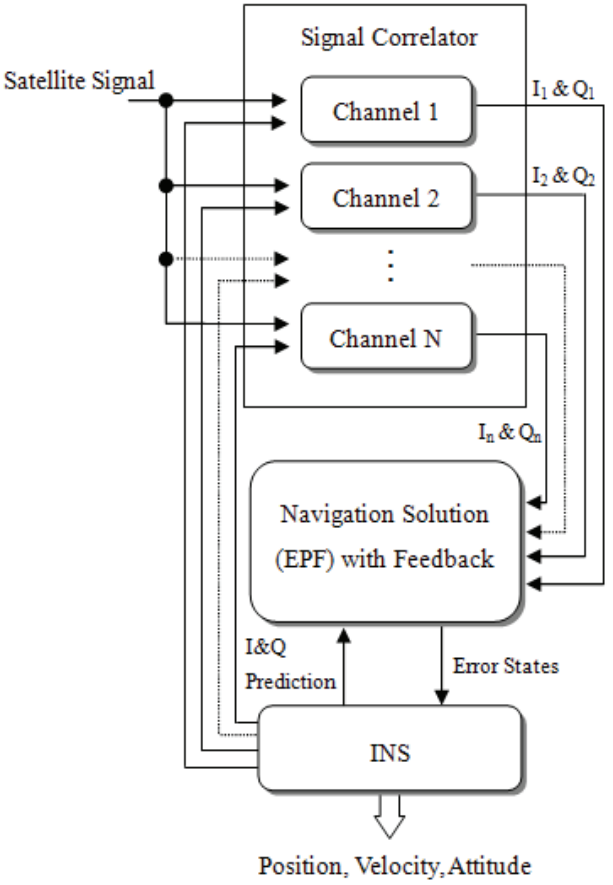

Figure 3: Illustration of the in-phase (I) and quadrature (Q) components as the measurements of the ultra-tightly coupled GPS/INS integration.

Substituting Eqs. (18) and (19) into Eq. (17), yields

$$y(t) = A \cdot CA(t) \cdot D(t) \cos(2\pi f t + \theta) + \eta, \tag{20}$$

where

$$P_L = |P_s(t_0 - \tau) - P_r(t_0)|, \tag{21}$$

$$V_L = \frac{d}{dt} |P_s(t_0 - \tau) - P_r(t_0)|, \tag{22}$$

$$f = f_0 - \frac{V_L f_0}{c}, \tag{23}$$

$$\theta = \theta_0 + \frac{2\pi f_0 t_0 V_L}{c} - \frac{2\pi f_0}{c} P_L. \tag{24}$$

The I and Q components of a satellite signal through the correlation can be written as

$$\begin{aligned} I &= \int_{kT}^{(k+1)T} \{\cos(\hat{\omega}t + \hat{\theta})[A\cos(\omega t + \theta) + \eta_0]\} dt \\ &= \frac{A}{2\omega_e}\{\sin(\omega_e(k+1)t + \theta_e) - \sin(\omega_e kt + \theta_e)\} + \eta_I \ , \end{aligned} \tag{25}$$

$$\begin{aligned} Q &= \int_{kT}^{(k+1)T} \{\sin(\hat{\omega}t + \hat{\theta})[A\cos(\omega t + \theta) + \eta_0]\} dt \\ &= \frac{-A}{2\omega_e}\{\cos(\omega_e(k+1)t + \theta_e) - \sin(\omega_e kt + \theta_e)\} + \eta_Q, \end{aligned} \tag{26}$$

where $\omega_e = \hat{\omega} - \omega = 2\pi(\hat{f} - f)$ is the frequency error tracked by the FLL, $\theta_e = \hat{\theta} - \theta$ is the phase error tracked by the PLL, k is the measurement epoch, T is the integration interval, and η_I and η_Q are the noise components. These error parameters f_e and θ_e are described in terms of the position and velocity as

$$f_e = \frac{f_0}{c}|\hat{V}_L - V_L|, \tag{27}$$

$$\theta_e = \frac{2\pi f_0}{c}(|\hat{V}_L - V_L|t - |\hat{P}_L - P_L|), \tag{28}$$

where P_L and V_L are the measured position and velocity of the receiver, respectively, and the $\hat{P}_L$ and $\hat{V}_L$ are the receiver estimates of the position and velocity, respectively.

4 The proposed fuzzy adaptive extended particle filter strategy

The process model of the extended particle filter is dependent on the dynamical characteristics of vehicle. It is well-known that poorly designed mathematical model for the EPF may lead to the divergence. The FLAS can be used to adapt the gain and prevent the particle filter from the divergence. In addition, the FLAS is employed to make the necessary trade-off between the accuracy and computational burden due to the increased dimension of the state vector and associated matrices.

In this paper, a Takagi-Sugeno (T-S) fuzzy logic system is used to detect the divergence of EPF and adapt the filter. The T-S fuzzy system represents the conclusion by functions.

A typical rule in the T-S model has the form:

IF Input x_1 is F_1^1 and Input x_2 is F_2^1 ... and Input x_n is F_n^1

THEN Output $y_k = f_k(x_1, x_2, \ldots, x_n) = C_{k0} + C_{k1}x_1 + \cdots + C_{kn}x_n$,

where $C_{ki}(i = 0 \sim n)$ are constants in the k-th rule. For the first-order model, we have the rule in the form:

IF Input x_1 is F_1^1 and Input x_2 is F_2^1

THEN Output $y_k = C_{10} + C_{11}x_1 + C_{12}x_2$,

where F_1^1 and F_2^1 are fuzzy sets and C_{10}, C_{11} and C_{12} are constants. For a zero-order model, the output level is a constant:

IF Input x_1 is F_1^1 and Input x_2 is F_2^1 THEN Output $y_k = C_{10}$.

The output is the weighted average of they_k:

$$y = \sum_{k=1}^{M} w_k . y_k, \tag{29}$$

where the weights w_k are computed as below:

$$w_k = \frac{\prod_{i=1}^{n} \mu_{F_i^k}(x_i)}{\sum_{j=1}^{M} \left[\prod_{i=1}^{n} \mu_{F_i^j}(x_i) \right]}. \tag{30}$$

The FLAS mechanism can be incorporated with determining the process noise covariance, leading to the proposed fuzzy adaptive extended particle filter (FAEPF). The FAEPF is composed of the FLAS and the EPF. Characteristics of the FLAS depend on the fuzzy rules and the effectiveness of rules directly influences its performance. The defuzzification is used to provide the deterministic value of a membership function for the output. Using the fuzzy logic to infer the consequent of a set of fuzzy production rules, it invariably leads to the fuzzy output subsets. The fuzzy modeling method describes characteristics of a system by utilizing the fuzzy inference rules.

The degree of divergence (DOD) parameters identifies the degree of change in vehicle dynamics and needs to be defined [Tseng and Jwo (2009), Jwo and Lai (2009)]. In this study, we present that an adaptive approach is given as follows. The innovation information at the present epoch is employed to timely reflect the change in the vehicle dynamics. The DOD parameter ξ can be defined as the trace of innovation covariance matrix at present epoch (i.e., the window size is one) and divided into

the number of satellites as follows:

$$\xi = \frac{1}{m}\sum_{i=1}^{m} \boldsymbol{\upsilon}_i \boldsymbol{\upsilon}_i^T, \tag{31}$$

where $\boldsymbol{\upsilon}_k = [\upsilon_1\ \upsilon_2 ... \upsilon_m]^T$, m is the number of measurements (number of signals from the receiver correlator, in-phase and quadrature). Furthermore, the averaged magnitude of innovation can also be used at the present epoch:

$$\zeta = \frac{1}{m}\sum_{i=1}^{m} |\upsilon_i|. \tag{32}$$

In the FLAS, the DOD parameters are employed to the inputs for the fuzzy inference engines. By monitoring the DOD parameters, we use the FLAS to on-line determine the process noise covariance of EPF according to the innovation information, and accordingly improve the performance in terms of tracking capability and the estimation accuracy. Besides, by using the adaptive adjustment of process noise covariance to ensure a rapid parameter convergence and to reduce the computational load of PF.

5 Numerical simulations and performance evaluation

The proposed fuzzy adaptive EPF scheme, UKF and EPF are carried out in the ultra-tightly coupled integrated navigation system processing. Fig. 4 shows the configuration of the ultra-tight integration processing on the basis of the FLAS-coupled EPF filtering mechanism. The simulation was conducted by a personal computer with Intel(R) 2 Dual CPU T7250 (2GHz). The commercial software Satellite Navigation (SATNAV) Toolbox with GPSoft LLC was employed to generate the satellite positions and pseudoranges. For the simulation of GPS, we consider the ionospheric delay, the tropospheric delay, the receiver noise and the multipath. The GPS signals for nine different satellites with PRN codes 3, 4, 6, 7, 9, 16, 18, 19, 21 were generated.

Using the differential equations, we can describe the two-dimensional inertial navigation state is as follows:

$$\begin{bmatrix} \dot{n} \\ \dot{e} \\ \dot{v}_n \\ \dot{v}_e \\ \dot{\psi} \end{bmatrix} = \begin{bmatrix} v_n \\ v_e \\ a_n \\ a_e \\ \omega_r \end{bmatrix} = \begin{bmatrix} v_n \\ v_e \\ \cos(\psi)a_u - \sin(\psi)a_v \\ \sin(\psi)a_u + \cos(\psi)a_v \\ \omega_r \end{bmatrix}, \tag{33}$$

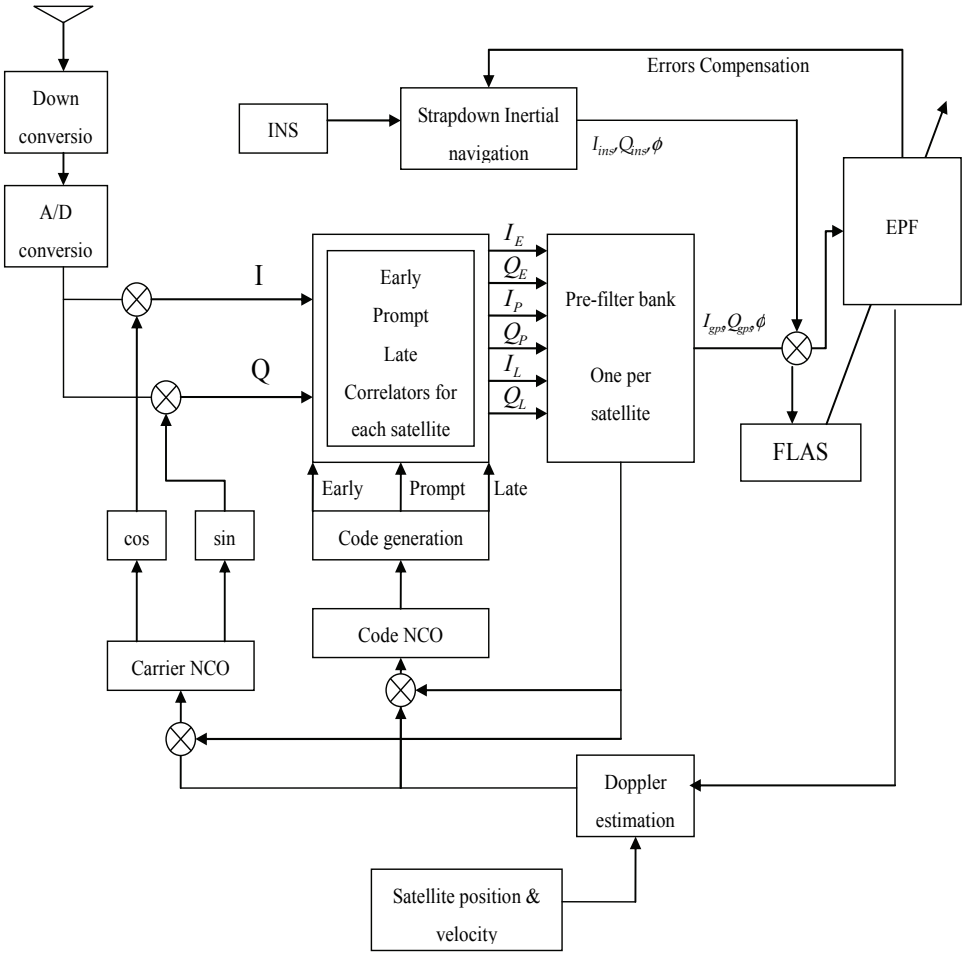

Figure 4: The configuration of the ultra-tight integration processing based on the FLAS-coupled EPF filtering mechanism.

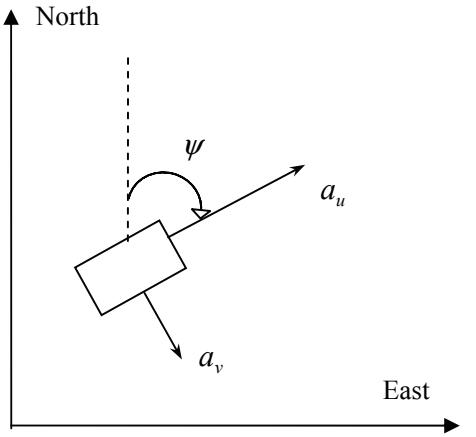

Figure 5: Illustration of the two-dimensional inertial navigation.

where $[a_u, a_v]$ are the measured acceleration in the body frame, and ω_r is the measured yaw rate in the body frame as shown in Fig. 5. The error model of INS is augmented by some sensor error states such as accelerometer biases and gyroscope drifts. In fact, there are several random errors associated with each inertial sensor. It is difficult to set a certain stochastic model for each inertial sensor that works efficiently at all environments and reflects the long-term behavior of sensor errors. By linearizing Eq. (33), we can acquire the following equation:

$$\frac{d}{dt}\begin{bmatrix}\delta n\\ \delta e\\ \delta v_n\\ \delta v_e\\ \delta \psi\\ \delta a_u\\ \delta a_v\\ \delta \omega_r\end{bmatrix} = \begin{bmatrix}0&0&1&0&0&0&0&0\\ 0&0&0&1&0&0&0&0\\ 0&0&0&0&-a_e&\cos(\psi)&-\sin(\psi)&0\\ 0&0&0&0&-a_n&\sin(\psi)&\cos(\psi)&0\\ 0&0&0&0&0&0&0&1\\ 0&0&0&0&0&0&0&0\\ 0&0&0&0&0&0&0&0\\ 0&0&0&0&0&0&0&0\end{bmatrix}\begin{bmatrix}\delta n\\ \delta e\\ \delta v_n\\ \delta v_e\\ \delta \psi\\ \delta a_u\\ \delta a_v\\ \delta \omega_r\end{bmatrix} + \begin{bmatrix}0\\ 0\\ u_{acc}\\ u_{acc}\\ u_{gyro}\\ u^b_{acc}\\ u^b_{acc}\\ u^b_{gyro}\end{bmatrix}, \tag{34}$$

which will be utilized in the integration navigation filter as the inertial error model. In Eq. (34), δn and δe represent the east and north position errors, respectively, δv_n and δv_e denote the east and north velocity errors respectively, $\delta \psi$ indicate yaw angle, and δa_u, δa_v and $\delta \omega_r$mean the accelerometer biases and gyroscope drift, respectively.

The measurement Jacobian matrix for the ultra-tightly coupled architecture is writ-

ten as

$$\mathbf{H}_k = \begin{bmatrix} h^1_{iy} & h^1_{ix} & h^1_{i\dot{y}} & h^1_{i\dot{x}} & 0 & 0 & 0 & 0 \\ h^1_{qy} & h^1_{qx} & h^1_{q\dot{y}} & h^1_{q\dot{x}} & 0 & 0 & 0 & 0 \\ \vdots & \vdots & \vdots & \vdots & \vdots & & & \\ h^n_{iy} & h^n_{ix} & h^n_{i\dot{y}} & h^n_{i\dot{x}} & 0 & & \vdots & \\ h^n_{qy} & h^n_{qx} & h^n_{q\dot{y}} & h^n_{q\dot{x}} & 0 & & & \\ 0 & 0 & 1 & 0 & 0 & & & \\ 0 & 0 & 0 & 1 & 0 & & \vdots & \\ 0 & 0 & 0 & 0 & 1 & 0 & 0 & 0 \end{bmatrix}, \tag{35}$$

where the matrix elements are

$$h^1_{ix} = \frac{1}{2}\left[\frac{\partial E[I]}{\partial \theta_e}\frac{\partial \theta_e}{\partial x} + \frac{\partial E[I]}{\partial w_e}\frac{\partial w_e}{\partial x}\right], h^1_{i\dot{x}} = \frac{1}{2}\left[\frac{\partial E[I]}{\partial \theta_e}\frac{\partial \theta_e}{\partial \dot{x}} + \frac{\partial E[I]}{\partial w_e}\frac{\partial w_e}{\partial \dot{x}}\right], \tag{36}$$

$$h^1_{qy} = \frac{1}{2}\left[\frac{\partial E[Q]}{\partial \theta_e}\frac{\partial \theta_e}{\partial y} + \frac{\partial E[Q]}{\partial w_e}\frac{\partial w_e}{\partial y}\right], h^1_{q\dot{y}} = \frac{1}{2}\left[\frac{\partial E[Q]}{\partial \theta_e}\frac{\partial \theta_e}{\partial \dot{y}} + \frac{\partial E[Q]}{\partial w_e}\frac{\partial w_e}{\partial \dot{y}}\right], \tag{37}$$

where h^1_{ix} is the vector that represents the east position with the I measurement tracked in channel 1, $h^1_{i\dot{x}}$ indicates the east velocity, h^1_{qy} is the vector that denotes the north position with the Q measurement tracked in channel 1, $h^1_{q\dot{y}}$ means the north velocity, and n is the number of the tracked satellites.

The membership functions (MFs) of input fuzzy variable DOD parameters as shown in Fig. 6, which mean the triangle MFs. In this paper, the presented FLAS is the *If-Then* form and consists of nine rules:

1. IF ξ is zero and ζ is zero THEN s is 1,
2. IF ξ is zero and ζ is small THEN s is 1,
3. IF ξ is zero and ζ is large THEN s is 1,
4. IF ξ is small and ζ is zero THEN s is $2\xi + 2\zeta + 4$,
5. IF ξ is small and ζ is small THEN s is $2\xi + 2\zeta + 4$,
6. IF ξ is small and ζ is large THEN s is $6\xi + 6\zeta + 12$,
7. IF ξ is large and ζ is zero THEN s is $6\xi + 6\zeta + 12$,
8. IF ξ is large and ζ is small THEN s is $6\xi + 6\zeta + 12$,

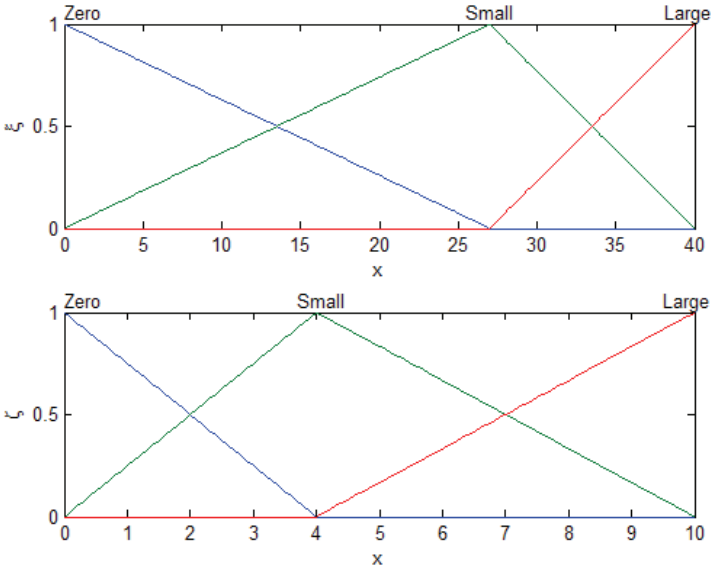

Figure 6: Membership functions of input fuzzy variables ξ (top) and ζ (bottom).

9. IF ξ is large and ζ is large THEN s is $6\xi + 6\zeta + 12$,

where s denotes the scale factor of the process noise covariance matrix in the EKF. To investigate the influence of high dynamic environments and GPS outages on the ultra-tight GPS/INS integration system performance, we present these two different experiments in the high dynamic environments and GPS signal blockages scenarios. First, the high-dynamic maneuvers can be described the motion dynamics of vehicle approximately. Second, investigating the performance during the period of GPS outage, we assume that the signal is blocked out during the time interval 701$\sim$1000 seconds.

5.1 Effect of the high dynamic environments on filters estimation

The experiment shows a simulated vehicle trajectory originating from the (0,0) m location in the ENU coordinate frame. The trajectories of the simulated vehicle (solid) and the unaided INS derived position (dashed) are shown in Fig. 7. The simulated sensor outputs for the accelerometers and gyroscope are shown as in Fig. 8. According to the dynamic characteristics, the vehicle is simulated to conduct constant-velocity (CV) straight-line during seven time intervals, 0-300, 501-600, 701-1000, 1101-1400, 1501-1600, 1701-1800 and 1901-2000s, all at a speed of 10π m/s. Furthermore, the higher dynamic maneuvering conducted

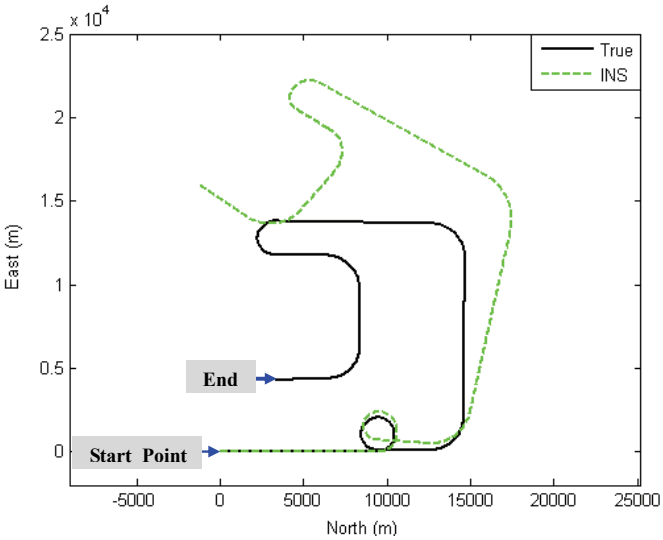

Figure 7: Trajectory of the high dynamic environments scenarios for the simulated vehicle (solid) and the INS derived position (dashed).

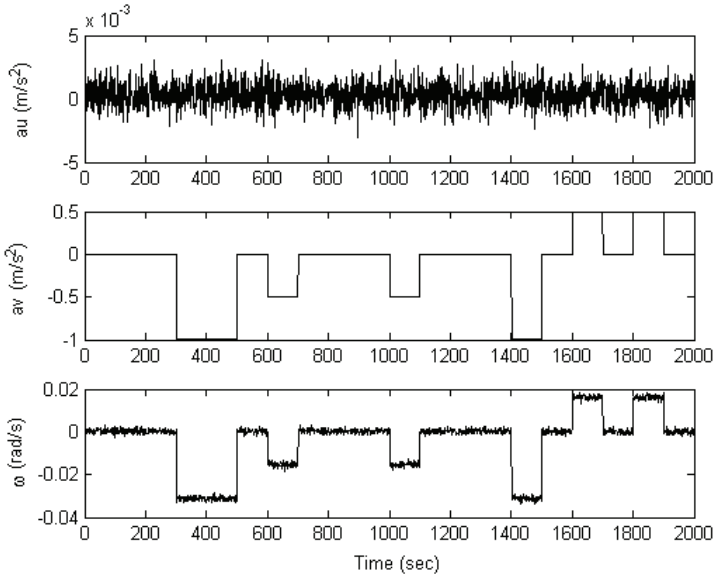

Figure 8: Simulated sensor outputs for the accelerometers and gyroscope. (From Fig. 7 trajectory data output)

counter-clockwise and clockwise circular/turn motion during 301-500, 601-700, 1001-1100, 1401-1500, 1601-1700 and 1801-1900s. The description of vehicle motion is listed in Table 1. The standard deviations of inertial sensors are 9×10^{-4} m/s^2 for accelerometers and gyroscopes, respectively.

Table 1: Description of the vehicle motion. (For the high dynamic environments scenarios)

Time interval (sec)	Motion
[0-300]	Constant velocity straight line
[301-500]	Circular motion
[501-600]	Constant velocity straight line
[601-700]	Counter-clockwise turn
[701-1000]	Constant velocity straight line
[1001-1100]	Counter-clockwise turn
[1101-1400]	Constant velocity straight line
[1401-1500]	Counter-clockwise turn
[1501-1600]	Constant velocity straight line
[1601-1700]	Clockwise turn
[1701-1800]	Constant velocity straight line
[1801-1900]	Clockwise turn
[1901-2000]	Constant velocity straight line

By using the UKF, EPF and FAEPF approaches, Figs. 9 to 11 show the navigation results for maneuvering vehicle under the high dynamic environments. Fig. 12 provides comparison of east and north position root mean squared errors via these three approaches: The UKF, EPF and FAEPF. Comparing the FAEPF with EPF, we find the FAEPF with only uses 50 particles performs better than the EPF with 100 particles. From these numerical results, several time intervals of the vehicle are maneuvering. Since the EPF can generate an approximate true probability density estimate of the system, the proposal distribution of EPF is closer to the true posterior distribution than the UKF. However, it requires a large number of particles to sample the high dimensional state space effectively, and increases the computational load.

The proposed fuzzy adaptive EPF has a good capability to detect the change in vehicle dynamics quickly and adjust the process noise covariance by monitoring the DOD parameters. The FLAS is able to on-line determine the process noise covariance of EPF, and prevents the divergence, and obtains the high navigation accuracy. Therefore, the FAEPF can successfully reduce the computational load, which does

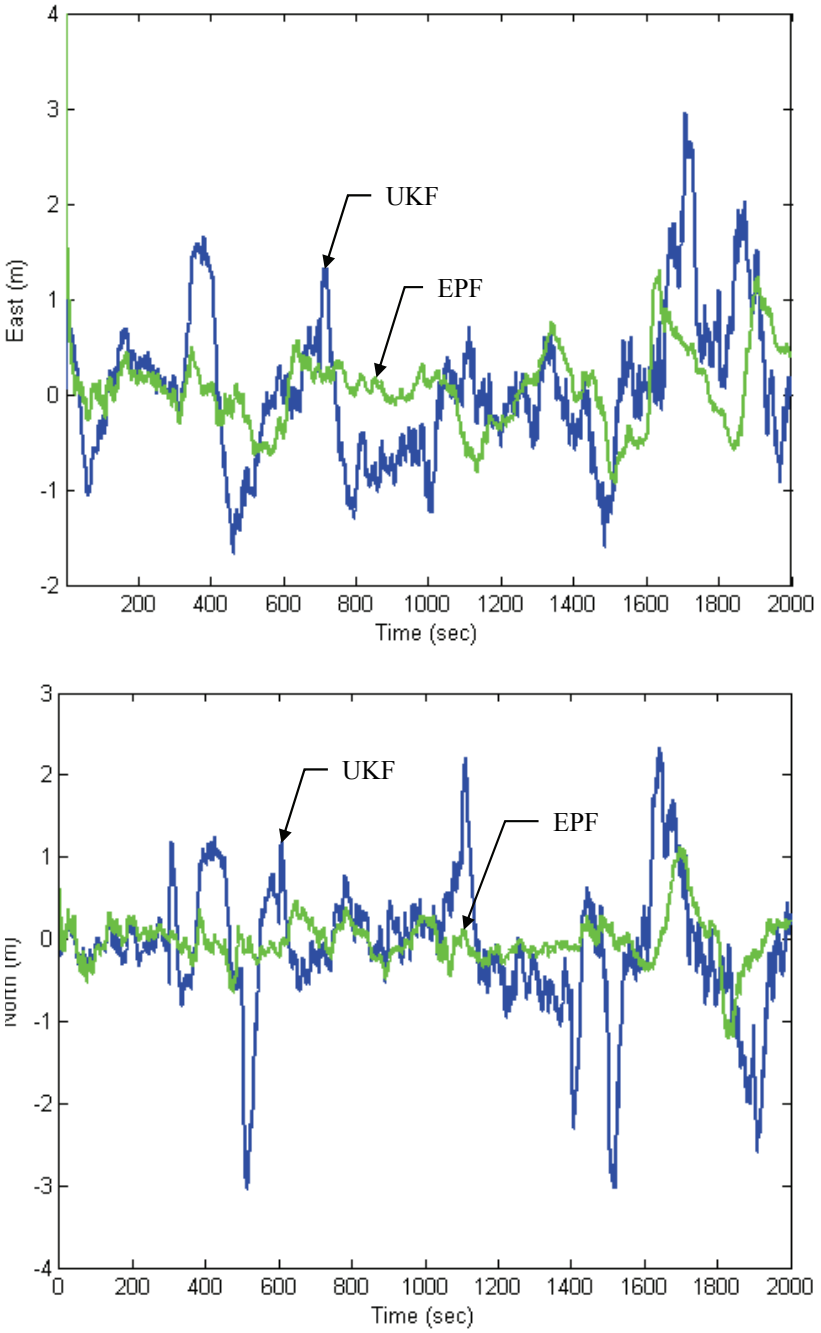

Figure 9: Comparison of the navigation accuracy for UKF and EPF in high dynamic environments.

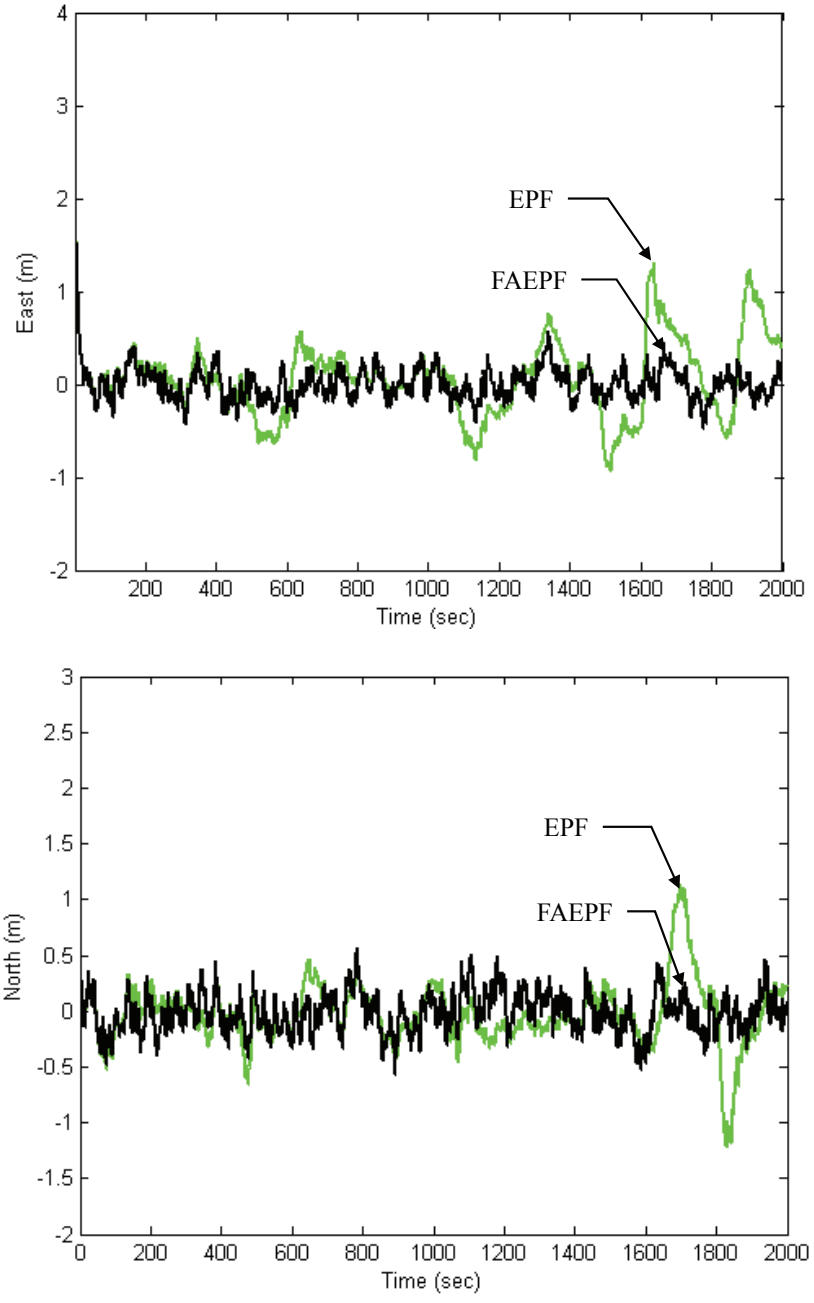

Figure 10: Comparison of the navigation accuracy for EPF and FAEPF in high dynamic environments.

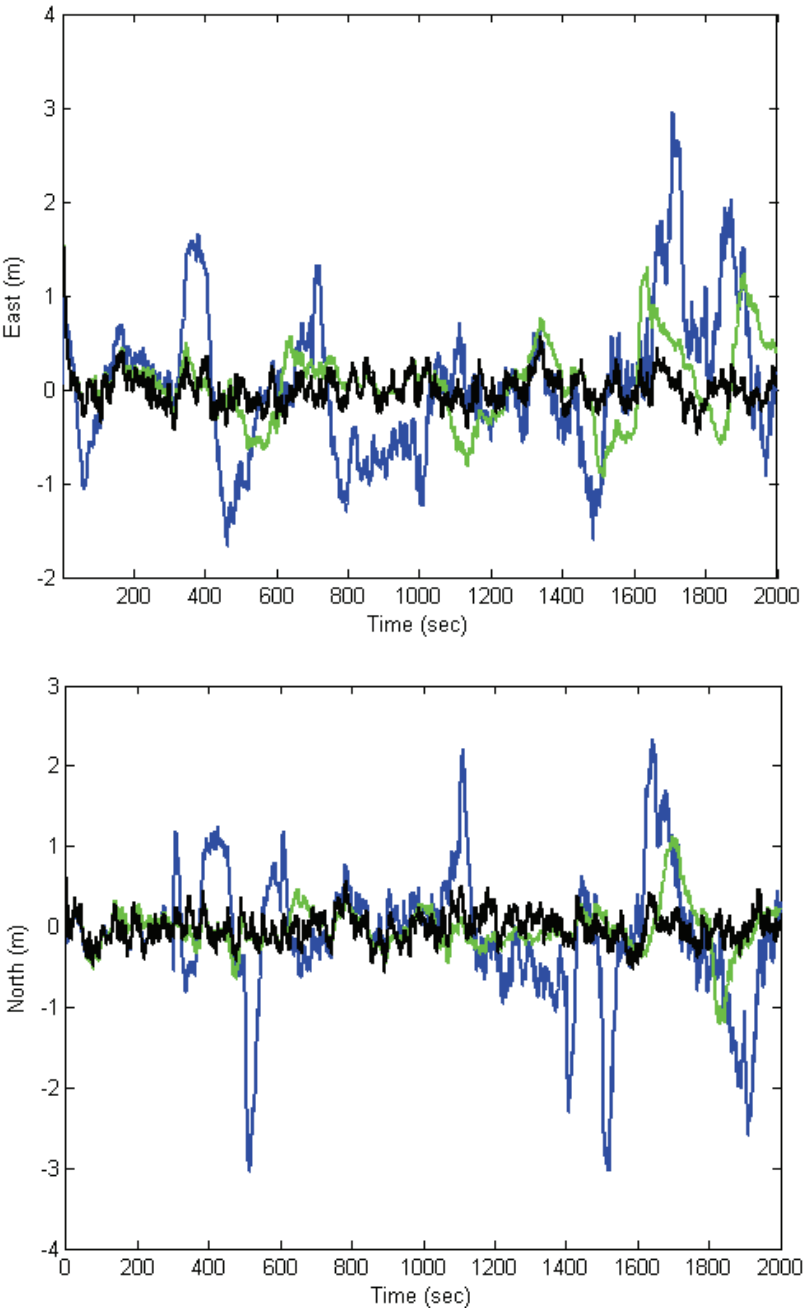

Figure 11: Comparison of the navigation accuracy for UKF, EPF and FAEPF in high dynamic environments. (FAEPF approach is the black line; EPF approach is the green line; UKF approach is the blue line)

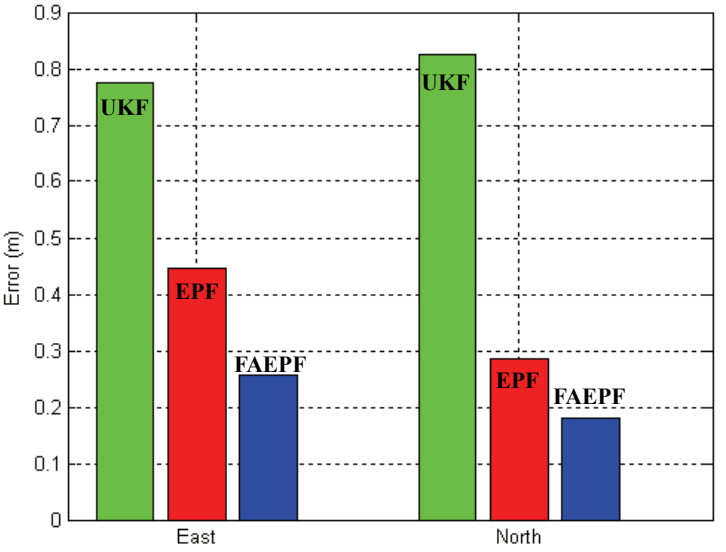

Figure 12: Comparison of east and north position RMS errors via UKF, EPF and FAEPF approaches for the high dynamic environments scenarios.

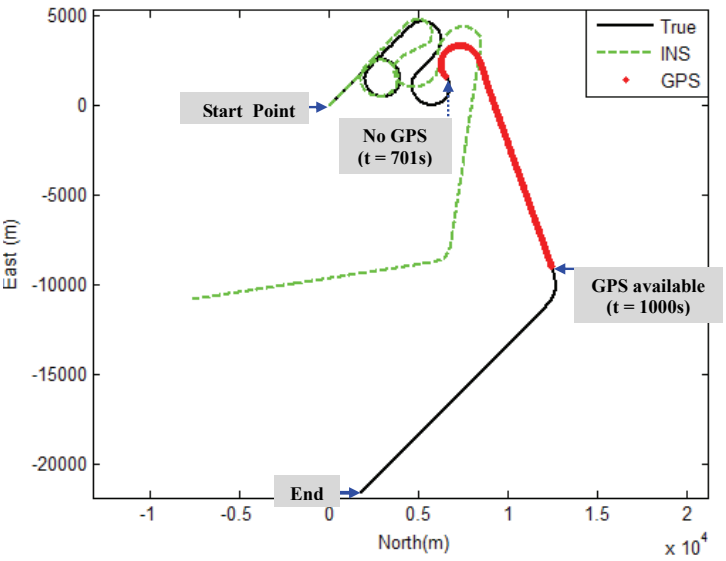

Figure 13: Trajectory for the simulated vehicle (solid) and the INS derived position (dashed), where GPS outages occur during 701 1000s.

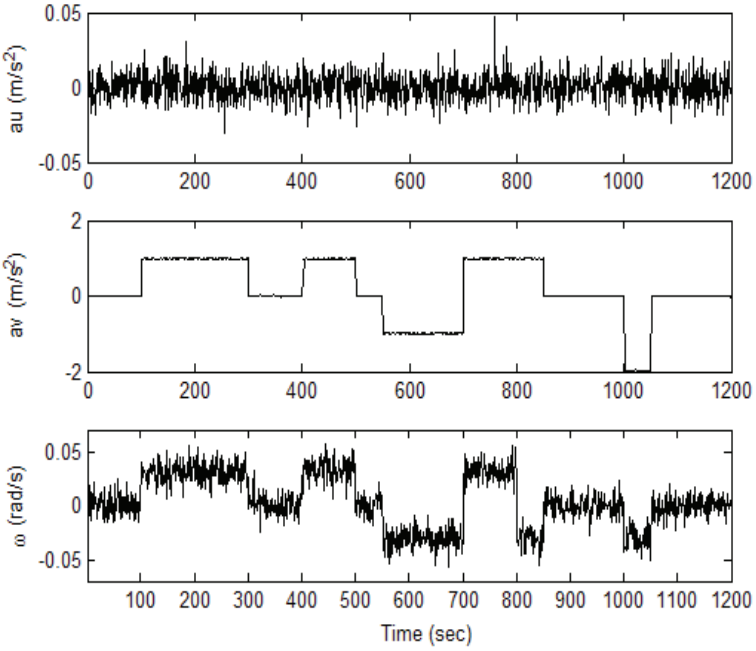

Figure 14: Simulated sensor outputs for the accelerometers and gyroscope. (From Fig. 13 trajectory data output)

not need an impractically large number of particles to sample the posterior density function.

Table 2: Description of the vehicle motion. (For the GPS outages scenarios)

Time interval (sec)	Motion
[0-100]	Constant velocity straight line
[101-300]	Circular motion
[301-400]	Constant velocity straight line
[401-500]	Clockwise turn
[501-550]	Constant velocity straight line
[551-700]	Counter-clockwise turn
[701-850]	Clockwise turn
[851-1000]	Constant velocity straight line
[1001-1050]	Clockwise turn
[1051-1200]	Constant velocity straight line

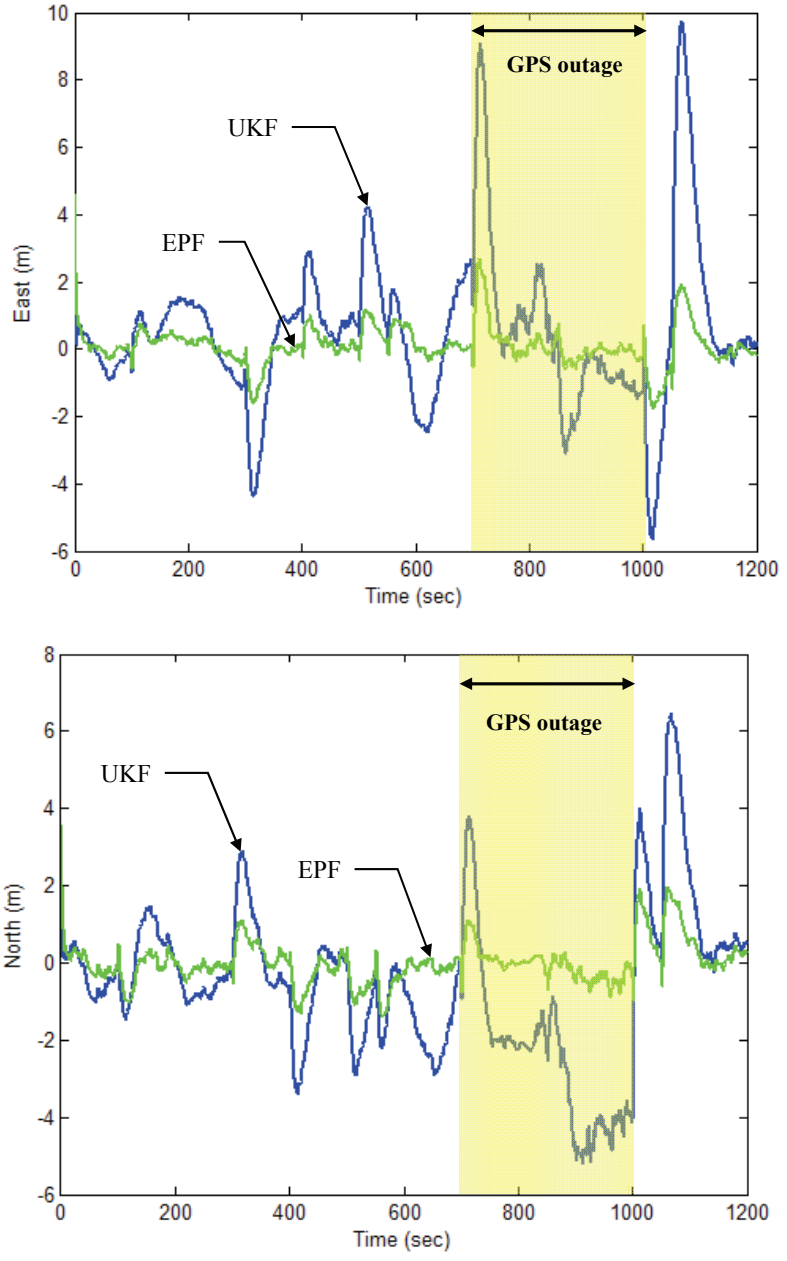

Figure 15: Comparison of positioning errors for UKF and EPF for GPS outages during 701∼1000 seconds.

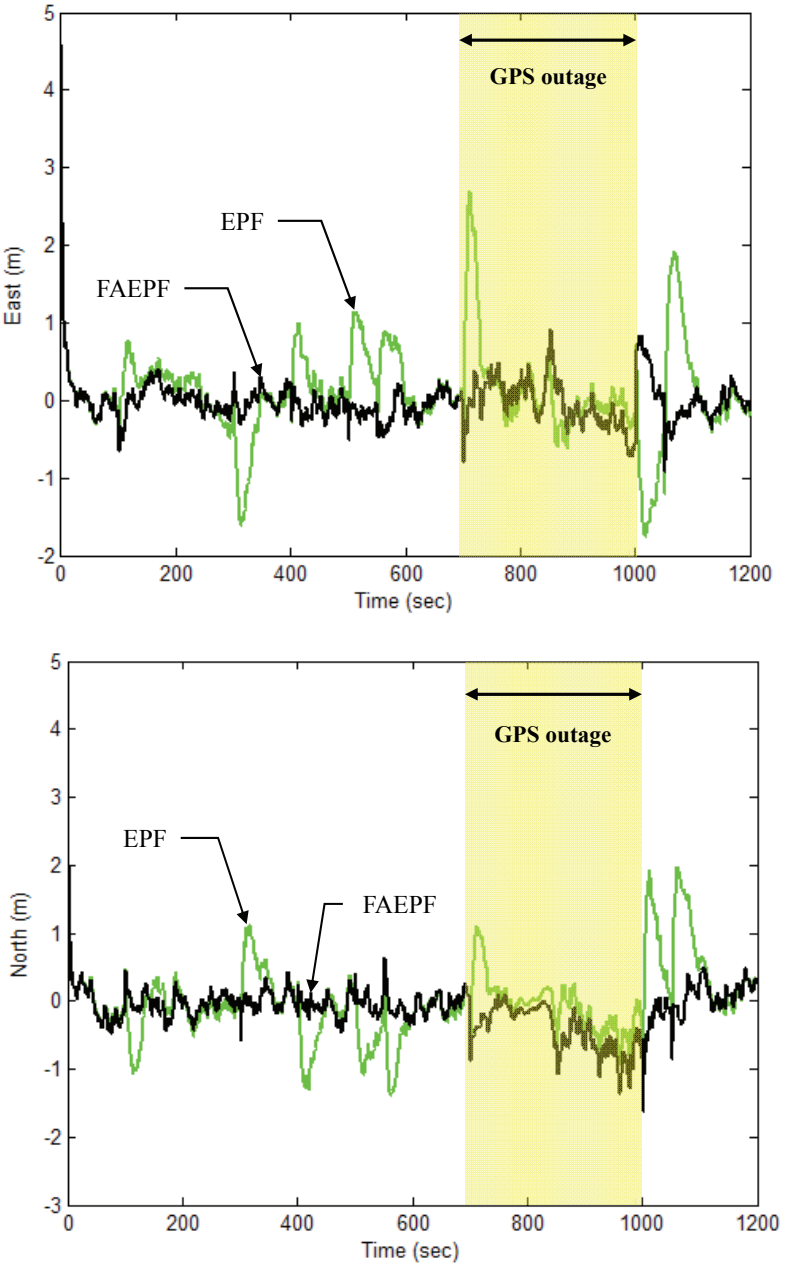

Figure 16: Comparison of positioning errors for EPF and FAEPF for GPS outages during 701∼1000 seconds.

701∼1000 seconds.

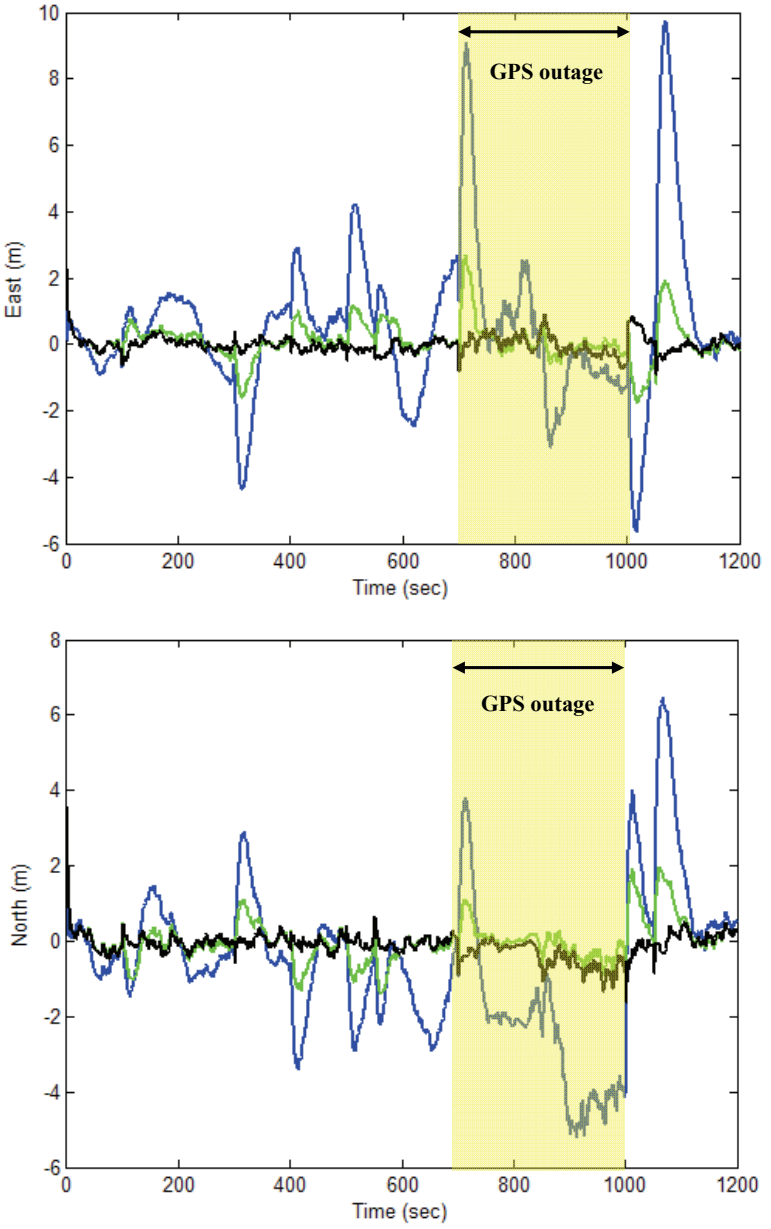

Figure 17: Comparison of positioning errors for UKF, EPF and FAEPF for GPS outages during 701∼1000 seconds. (FAEPF approach is the black line; EPF approach is the green line; UKF approach is the blue line)

5.2 Navigation performance during the GPS outages

Figs. 15-17 show the effect of vehicle dynamics with the navigation error estimation in several nonlinear filters during the GPS outages. Trajectories of the simulated vehicle (solid) and the unaided INS derived position (dashed) are shown in Fig. 13. The simulated sensor outputs for the accelerometers and gyroscope are shown as in Fig. 14. Moreover, the description of vehicle motion is listed in Table 1. The simulated GPS signal blockages occur from 701s to 1000s. In this time interval, the vehicle also experiences two dynamic categories (i.e., clockwise turn during 701-850s and constant velocity straight line motion during 851-1000s). From the above simulation, comparing Figs. 15 and 16 with three different nonlinear filters under the vary scenario. During these periods (300 seconds), the navigation filter only uses the inertial sensors measurement to correct the trajectory of vehicle since the navigation data are disconnected. Note that the positioning errors of the EPF and FAEPF are reduced remarkably. Besides, these two filters can improve the fast acquisition, track the signal in the ultra-tightly coupled integration, and maintain the navigation estimation accuracy as compared with the UKF approaches. However, the above mention discussion that the proposed FAEPF employs the FLAS to automatically adjust the process noise covariance while the FLAS timely detects the increase of DOD parameter. As a result, the proposed FAEPF approach on the basic of the GPS signal blockage is effective to reduce the divergence errors in the navigation processing and to decrease the computational load. Fig. 18 provides the comparison of east and north position errors via all these three different approaches: The UKF, EPF and FAEPF.

6 Conclusions

This paper proposed a fuzzy adaptive extended particle filter for the ultra-tight GPS/INS navigation processing to prevent the divergence problem in the high dynamic environments and periods of the partial GPS shading. The extended particle filter has good potential for the ultra-tightly coupled GPS/INS integrated navigation system. Unlike the relatively traditional designs adopt the loosely or tightly coupled integration architectures, the ultra-tight GPS/INS architecture involving the fusion of I (in-phase)and Q (quadrature) variables from the correlator of a GPS receiver with the INS. The EPF can efficiently deal with the non-linear and/or non-Gaussian problem, where the EKF is used to generate the proposal distribution and leads to the remarkable accurate estimation. However, it requires an impractically large number of particles to sample the state space effectively, and costs a lot of the computational load.

In this study, the fuzzy logic system is employed to improve the EPF performance.

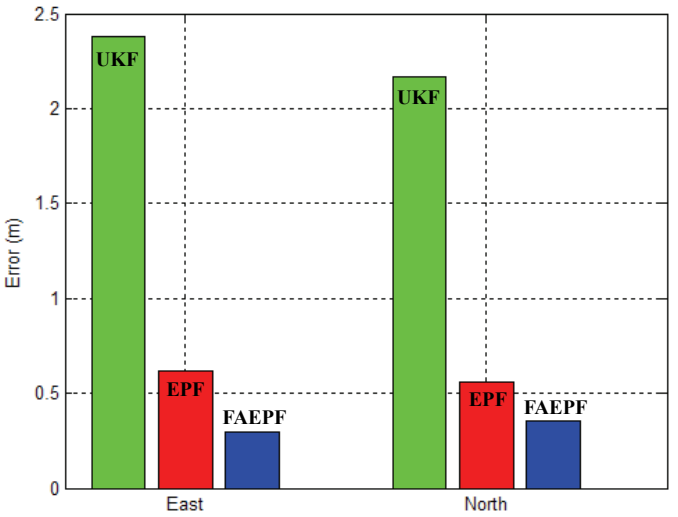

Figure 18: Comparison of east and north position RMS errors via UKF, EPF and FAEPF approaches for the GPS outages scenarios.

The FLAS is incorporated into the EPF and the fuzzy logic as a mechanism, which detects the dynamical changes and implements the on-line determination of process noise covariance. By monitoring the innovative information, we can obtain the good performance. Comparing the performance of UKF and EPF, the proposed FAEPF approach demonstrates very accurate results and low computational load under the high dynamic environments during the GPS outages.

Acknowledgement: The first author thanks Professor Dah-Jing Jwo to give suggestions and help. Besides, the corresponding author would like to express his thanks to the National Science Council, ROC, for their financial supports under Grant Number NSC 98-2221-E-019-021-MY3.

References

Aggarwal, P.; Gu, D.; El-Sheimy, N. (2007): Extended particle filter (EPF) for land vehicle navigation applications. *IGNSS*, Sydney, Australia, pp. 4–6.

Arulampalan, S.; Maksell, S.; Gordon, N.; Clapp, T. (2002): A tutorial of particle filters for online nonlinear/non-Gaussian Bayesian tracking. *IEEE Trans. Signal Processing,* vol. 50, pp. 174–188.

Babu, R.; Wang, J. (2004): Improving the quality of IMU-derived doppler esti-

mates for ultra-tight GPS/INS integration. *GNSS Conf.*, Rotterdam, Netherlands, May, 16–19.

Babu, R.; Wang, J. (2009): Ultra-tight GPS/INS/PL integration: a system concept and performance analysis. *GPS Solut.*, vol. 13, pp. 75–82.

Boucher, C.; Noyer, J.-C. (2010): A hybrid particle approach for GNSS applications with partial GPS outages. *IEEE Trans. Instrum. Measurement*, vol. 59, pp. 498–505.

Brown, R.; Hwang, P. (1997): Introduction to Random Signals and Applied Kalman Filtering. New York: John Wiley & Sons.

Carpenter, J.; Fearnhead, P.; Clifford, P. (1999): Improved particle filter for nonlinear problems. *IEE Proc.-Radar, Sonar Navig.*, pp. 2–7.

Crassidis, J. L. (2006): Sigma-point Kalman filtering for integrated GPS and inertial navigation. *IEEE Trans. Aerosp. Electronic System*, vol. 42, no. 2, pp. 750–756.

Doucet, A.; Godsill, S. J.; Andrieu, C. (2000): On sequential simulation-based methods for Bayesian filtering. *Stat. Comput.*, vol. 10, pp. 197–208.

Doucet, A.; Freitas, N. De; Gordon, N. (2001): Sequential Monte Carlo Methods in Practice. USA: Springer Verlag New York Inc.

Farrell, J.; Barth, M. (1999): The Global Positioning System and Inertial Navigation, New York: McCraw-Hill.

Gelb, A. (1997): Applied Optimal Estimation. MA: M.I.T. Press.

Gordon, N.; Ristic, B.; Arulampalam, S. (2004): Beyond the Kalman Filter : Particle Filter for Tracking Applications. Artech House, Boston.

Julier, S. J. (2002): The scaled unscented transformation. *ACC*, Anchorage, USA, pp. 4555–4559.

Julier, S. J.; Uhlmann, J. K. (2002): Reduced sigma point filters for the propagation of means and covariances through nonlinear transformations. *ACC*, Anchorage, USA, pp. 887–892.

Julier, S. J.; Uhlmann, J. K.; Durrant, H. F. (1995): A new approach for filtering nonlinear systems. *ACC*, pp. 1628–1632.

Julier, S. J.; Uhlmann, J. K.; Durrant, H. F. (2000): A new approach for nonlinear transformations of means and covariances in filters and estimators. *IEEE Trans. Automatic Control*, vol. 45, pp. 477–482.

Jwo, D. J.; Lai, C. N. (2009): Navigation Integration Using the Fuzzy Strong Tracking Unscented Kalman Filter. *J. Navig.*, vol. 62, no. 2, pp. 303–322.

Lerro, D.; Shalom, Y. (1995): Tracking with debaised consistent converted mea-

surements versus EKF. *IEEE Trans. Aerosp. Electronic System*, vol. 29, pp. 1015–1022.

Li, Y.; Wang, J.; Rizos, C.; Mumford, P. J.; Ding, W. (2006): Low-cost tightly coupled GPS/INS integration based on a nonlinear Kalman filter design. *The U.S. ION Tech*., Meeting, pp. 958–966.

Noureldin, A.; Karamat, T. B.; Eberts, M. D.; El-Shafie, A. (2009): Performance enhancement of MEMS based INS/GPS integration for low cost navigation applications. *IEEE Trans. Veh. Tech.*, vol. 58, pp. 1077–1096.

Salychev, O. (1998): Inertial Systems in Navigation and Geophysics, Moscow: Bauman MSTU.

Tseng, C. H.; Jwo, D. J. (2011): Designing fuzzy adaptive nonlinear filter for land vehicle ultra-tightly coupled integrated navigation sensor fusion. *Sensors and Transducers*, vol. 128, pp. 1–16.

Wang, X. L.; Li, Y. F. (2011): An innovative scheme for SINS/GPS ultra-tight integration system with low-grade IMU. *Aerosp. Sci. Tech.*, In Press.

Won, S.-H. P.; Melek, W. W.; Golnaraghi, F. (2010): A Kalman/particle filter-based position and orientation estimation method using a position sensor/inertial measurement hybrid system. *IEEE Trans. Ind. Electron.*, vol. 57, no. 5, pp. 1787–1798.

Yu, J.; Wang, X.; Ji, J. (2010): Design and analysis for an innovative scheme of SINS/GPS ultra-tight integration. *Aircraft Eng. Aerosp. Tech.*, vol. 82, pp. 4–14.

Yuan, G.; Zhang, T. (2009): Unscented Kalman Filtering for Ultra-tightly Coupled GPS/INS Integration. *IEEE ICMA*, Changchun, China, Aug. 9–12, pp. 4556–4560.